





## Article

# Non-Invasive Prediction of Site-Specific Coronary Atherosclerotic Plaque Progression using Lipidomics, Blood Flow, and LDL Transport Modeling

Antonis I. Sakellarios<sup>1,2</sup>, Panagiota Tsompou<sup>1,2</sup>, Vassiliki Kigka<sup>1,2</sup>, Panagiotis Siogkas<sup>1,2</sup>, Savvas Kyriakidis<sup>1</sup>, Nikolaos Tachos<sup>1</sup>, Georgia Karanasiou<sup>1</sup>, Arthur Scholte<sup>3</sup>, Alberto Clemente<sup>4</sup>, Danilo Neglia<sup>4</sup>, Oberdan Parodi<sup>5</sup>, Juhani Knuuti<sup>6</sup>, Lampros K. Michalis<sup>7</sup>, Gualtiero Pelosi<sup>5</sup>, Silvia Rocchiccioli<sup>5,\*</sup> and Dimitrios I. Fotiadis<sup>1,2,\*</sup>

- <sup>1</sup> Department of Biomedical Research, Institute of Molecular Biology and Biotechnology—FORTH, University Campus of Ioannina, GR45110 Ioannina, Greece; ansakel13@gmail.com (A.I.S.); panagiota.tsompou@gmail.com (P.T.); kigkavaso@gmail.com (V.K.); psiogkas4454@gmail.com (P.S.); savvasik21@gmail.com (S.K.); ntachos@gmail.com (N.T.); g.karanasiou@gmail.com (G.K.)
- <sup>2</sup> Unit of Medical Technology and Intelligent Information Systems, Department of Materials Science and Engineering, University of Ioannina, GR45110 Ioannina, Greece
- <sup>3</sup> Department of Cardiology, Leiden University Medical Center, 2333 ZA Leiden, The Netherlands; a.j.h.a.scholte@lumc.nl
- <sup>4</sup> Fondazione Toscana G. Monasterio, 56124 Pisa, Italy; clemente@ftgm.it (A.C.); dneiglia@ftgm.it (D.N.)
- <sup>5</sup> Institute of Clinical Physiology, National Research Council, 56124 Pisa, Italy; oberdan.parodi@virgilio.it (O.P.); pelosi@ifc.cnr.it (G.P.)
- <sup>6</sup> Turku PET Centre, University of Turku, Turku University Hospital, 20520 Turku, Finland; juhani.knuuti@tyks.fi
- <sup>7</sup> Department of Cardiology, Medical School, University of Ioannina, GR45110 Ioannina, Greece; lamprosmichalis@gmail.com
- \* Correspondence: silvia.rocchiccioli@ifc.cnr.it (S.R.); fotiadis@uoi.gr (D.I.F.); Tel.: +39-050-3153093 (S.R.); +30-26510-09006 (D.I.F.)



**Citation:** Sakellarios, A.I.; Tsompou, P.; Kigka, V.; Siogkas, P.; Kyriakidis, S.; Tachos, N.; Karanasiou, G.; Scholte, A.; Clemente, A.; Neglia, D.; et al.

Non-Invasive Prediction of Site-Specific Coronary Atherosclerotic Plaque Progression using Lipidomics, Blood Flow, and LDL Transport Modeling. *Appl. Sci.* **2021**, *11*, 1976. <https://doi.org/10.3390/app11051976>

Academic Editor: Andrea Ballini

Received: 2 January 2021

Accepted: 19 February 2021

Published: 24 February 2021

**Publisher's Note:** MDPI stays neutral with regard to jurisdictional claims in published maps and institutional affiliations.



**Copyright:** © 2021 by the authors. Licensee MDPI, Basel, Switzerland. This article is an open access article distributed under the terms and conditions of the Creative Commons Attribution (CC BY) license (<https://creativecommons.org/licenses/by/4.0/>).

**Abstract:** Background: coronary computed tomography angiography (CCTA) is a first line non-invasive imaging modality for detection of coronary atherosclerosis. Computational modeling with lipidomics analysis can be used for prediction of coronary atherosclerotic plaque progression. Methods: 187 patients (480 vessels) with stable coronary artery disease (CAD) undergoing CCTA scan at baseline and after  $6.2 \pm 1.4$  years were selected from the SMARTool clinical study cohort (Clinicaltrial.gov Identifiers NCT04448691) according to a computed tomography (CT) scan image quality suitable for three-dimensional (3D) reconstruction of coronary arteries and the absence of implanted coronary stents. Clinical and biohumoral data were collected, and plasma lipidomics analysis was performed. Blood flow and low-density lipoprotein (LDL) transport were modeled using patient-specific data to estimate endothelial shear stress (ESS) and LDL accumulation based on a previously developed methodology. Additionally, non-invasive Fractional Flow Reserve (FFR) was calculated (SmartFFR). Plaque progression was defined as significant change of at least two of the morphological metrics: lumen area, plaque area, plaque burden. Results: a multi-parametric predictive model, including traditional risk factors, plasma lipids, 3D imaging parameters, and computational data demonstrated 88% accuracy to predict site-specific plaque progression, outperforming current computational models. Conclusions: Low ESS and LDL accumulation, estimated by computational modeling of CCTA imaging, can be used to predict site-specific progression of coronary atherosclerotic plaques.

**Keywords:** prediction of plaque progression; computational modeling; endothelial shear stress; LDL transport; non-invasive FFR

## 1. Introduction

Coronary artery disease (CAD) clinical manifestations are one of the most common causes of death worldwide [1]. Cardiovascular risk factors and systemic lipid profiles are known to be associated with development of CAD. Reliable interpretation of coronary angiography using coronary computed tomography angiography (CCTA) requires sophisticated knowledge of normal coronary artery anatomy, pathophysiology of coronary artery atherosclerosis and congenital anomalies, characteristic features of coronary artery disease and its CCTA representation, the technology used and its limitations, the use of heart-specific three-dimensional interpretation software, and the ability to identify and overcome image artifacts in the available image dataset [2]. Computational modeling of invasive coronary imaging has been recently employed to investigate CAD pathophysiology and, in particular, the possible relationship between low endothelial shear stress (ESS) and plaque progression [3,4]. CCTA derived blood flow modeling and imaging characteristics were also recently used for the development of non-invasive predictive models of disease progression [5,6].

Besides blood rheology, computational modeling was recently used to describe the lipid accumulation in the arterial wall [7,8], which, in their majority, are in agreement with experimental findings [9]. The deployment of these models in a patient's database demonstrated that high accumulation of low-density lipoprotein (LDL) particles in the arterial wall is a predictor of disease progression [10].

The possible interaction of clinical risk factors and lipid profile with CCTA imaging characteristics as well as the combination of computational modeling of blood rheology with LDL transport and accumulation have not yet been investigated, with the aim of developing predictive models of coronary plaque progression. We hypothesized that combining systemic cardiovascular risk factors with local imaging and modeling characteristics in a multi-level model could help identify which arterial site, within the whole coronary tree, is more likely to undergo plaque formation/growth in a single patient with a given generic atherosclerosis progression risk. To this purpose, we examined, for the first time, the combined effect of lipidomics derived biomarkers and computational modeling of coronary arteries in 187 patients, with low to medium CAD risk, recruited in the H2020 SMARTool clinical study. Data were collected at two time points with an interscan period of  $6 \pm 2$  years. ESS calculation, estimation of LDL transport, and non-invasive Fractional Flow Reserve (FFR) calculation was performed to 480 vessels.

## 2. Materials and Methods

### 2.1. Study Design

A prospective, multicenter study in patients who underwent serial coronary CTA was conducted during the H2020 SMARTool project (Clinicaltrial.gov Identifiers NCT04448691) [11]. White patients were included by 7 centers from 5 European countries. The study protocol was approved by all local ethical committees, all patients gave their written informed consent to participate in the study, and the procedures followed were in accordance with institutional guidelines. Patients who previously underwent coronary CCTA for suspected CAD, as part of the Evaluation of Integrated Cardiac Imaging for the Detection and Characterization of Ischemic Heart Disease (EVINCI); FP7-222915;  $n = 152$ ) [12] or ARTreat (FP7-224297;  $n = 18$ ) [13] clinical studies, were prospectively included to undergo follow-up coronary CTA. Additionally, patients who underwent coronary CCTA in the period 2009 to 2012 for clinical indications ( $n = 32$ ) and were not originally included in the EVINCI and ARTreat studies were also prospectively included. A full list of inclusion and exclusion criteria is provided in the Supplementary Materials. Among the final SMARTool population, consisting of 263 patients, 187 patients were selected for this study based on the image quality of baseline CCTA as well as on the existence of stented arteries as shown in the Figure 1. For each patient, clinical risk factors, biohumoral variables, and lipidomics data had been collected, and CCTA examination was performed

at two time points, i.e., at baseline and at follow-up (mean follow-up  $6.22 \pm 1.42$  years, range of follow-up period: 1.86–11.3 years).

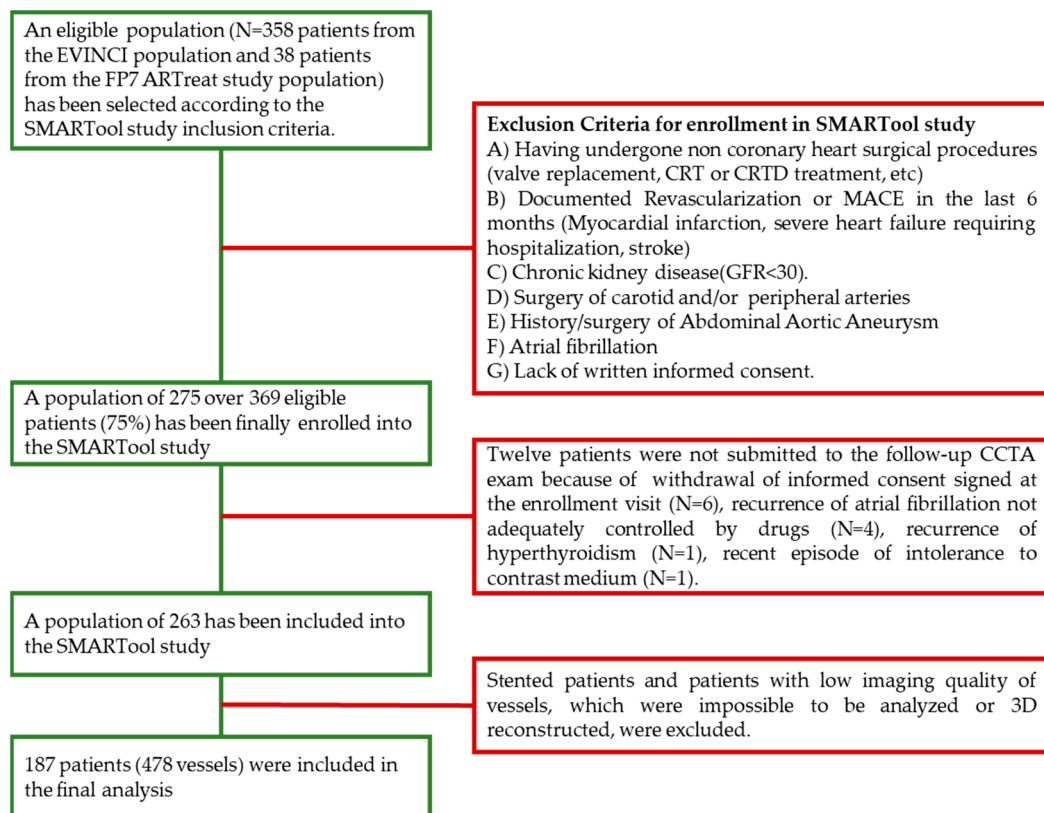


**Figure 1.** Inclusion and exclusion criteria of the current study.

## 2.2. Lipidomics Analysis

Plasma samples of all patients, stored at  $-80^{\circ}\text{C}$ , were thawed at room temperature and immediately subjected to lipid extraction and analysis. Total lipid extraction from an aliquot of plasma was performed according to Folch procedure [14]. Calibration standard and plasma sample analysis was performed by liquid chromatography–electrospray ionization–tandem mass spectrometry. Different volumes of calibration Standards (STDs)/plasma samples were injected:  $0.5\ \mu\text{L}$  for STDs 1,2-phosphatidyl ethanolamine: PE(15:0)(15:0) and Ceramides: Cer(d18:1/17:0);  $0.1\ \mu\text{L}$  for STDs cholesterol esters: CE(17:0), Triacyl glycerol: TG(17:0/17:0/17:0), sphingomyelin: SM(d18:1/16:0), and 1,2-phosphatidyl choline: PC(17:0)(17:0);  $0.5\ \mu\text{L}$  for plasma samples, as such, and  $0.1\ \mu\text{L}$  for plasma samples diluted 5-fold to avoid mass spectrometer saturation, due to the high concentration levels of these lipid species in plasma. Each injection was repeated in triplicate for each lipid standard to evaluate the reproducibility of the procedure. Lipid species absolute concentrations were calculated considering their area ratio (lipid peak area/internal Standards (ISTD) peak area) and interpolating it within the calibration curve of the corresponding external standard. MultiQuant 2.1 software (SCIEX, Concord, Canada) was used for lipid quantification. The lipids structures are presented in Annex 1.

## 2.3. CCTA Analysis and Three-Dimensional (3D) Reconstruction

In each of the 187 patients included in the current study, the right coronary artery (RCA), the left anterior descending artery (LAD), and the left circumflex artery (LCx) were analyzed. Baseline and follow-up CCTA scans were co-registered using landmarks, such as the bifurcations and calcified objects. Three-dimensional (3D) reconstruction of the

coronary lumen and outer vessel wall was performed using an in-house software, which provided measurements of lumen area, plaque area and plaque burden as previously described and validated by intravascular ultrasound – virtual histology (IVUS-VH) and manual annotations (11). RCA was reconstructed as a single arterial segment, while the left main was reconstructed, including the LAD and LCx as side branches.

#### 2.4. Blood Flow, LDL Transport Modeling, and Non-Invasive FFR Calculation

The finite element method was employed for modeling blood flow and LDL transport in the baseline CCTA 3D reconstructed geometries. A previously employed methodology is implemented for the solution of the Navier-Stokes equations [5]. ESS is calculated as the product of the shear rate at the endothelial membrane and the blood viscosity ( $\mu$ ) [15]. The modeling of LDL transport is achieved by solving the convection-diffusion equations in the lumen and the arterial wall. The patient-specific LDL blood concentration values at baseline blood tests was applied at the inlet of the geometries. Moreover, the patient-specific baseline blood pressure values were used to account for the effects of different pressure on the accumulation of LDL particles. The full details of the methodology have been reported elsewhere [7]. The SmartFFR calculation process and validation results have been previously described [16]. Briefly, a transient blood flow simulation of an increasing flow rate was used (i.e., 0 to 4 mL/s) to calculate the ratio of distal to proximal pressure over the examined coronary segment for the aforementioned flow range, normalized by the ratio over this range for a completely healthy arterial segment, providing a measure of hemodynamic significance, which is numerically equivalent to the average of the computed pressure ratio over this flow range.

#### 2.5. Statistics

For the analysis, we divided the arterial segments into 3 mm segments, which allows the association of plaque progression with computational results. We have calculated for each 3mm segment the lumen area, the plaque area, the plaque burden. The local ESS (defined as the minimum averaged ESS in an arc of 90°) and the LDL concentration value (defined as the maximum averaged LDL concentration in an arc of 90°) were calculated. The computationally calculated LDL concentration is presented normalized by the patient-specific serum LDL concentration (dimensionless). A single value of SmartFFR per vessel was defined. Besides these vascular variables, patient specific cardiovascular risk factors, circulating biohumoral markers, and lipid species from lipidomics analysis were entered in the statistical models. Baseline imaging characteristics, calculated ESS and LDL concentration values, and the patients' clinical and biohumoral data were associated with the progression of CAD, employing linear regression analysis. The associated variables ( $p < 0.1$ ) were entered in a multivariate model considering potential co-linearity between the variables. Variables with >50% missing values were excluded from the analysis. Independent predictors of CAD progression were assessed by a randomized multi-level mixed binary regression model. A receiver operating characteristic (ROC) curve analysis was implemented for the transformation of continuous variables to binary. Data analysis was performed using the SAS version 9.3 (SAS Institute). A  $p$ -value  $< 0.05$  was considered statistically significant.

### 3. Results

Baseline demographical and clinical characteristics of the study population are summarized in Table 1.

**Table 1.** Baseline demographics, clinical and biohumoral data.

	All Patients (N = 187)
Age (years)	60.73 ± 8.11
Gender (male)	107 (57.2%)
BMI	27.31 ± 3.52
Current smoker	25 (13.4%)
Family history of CAD	92 (49.2%)
<b>Risk factors</b>	
Diabetes mellitus	27 (14.4%)
Hypertension	111 (59.4%)
Dyslipidemia	127 (67.9%)
Obesity	33 (17.6%)
<b>Clinical presentation *</b>	
Atypical angina	86 (46.0%)
Typical angina	48 (25.7%)
Other symptoms	22 (11.8%)
No symptoms	12 (6.4%)
<b>Imaging presentation</b>	
No CAD	47 (25.1%)
Non-obstructive CAD	113 (60.4%)
Obstructive CAD	27 (14.4%)
<b>Biohumoral data</b>	
Total cholesterol	190.60 ± 49.50
Low density lipoprotein (LDL) cholesterol	114.09 ± 42.39
High density lipoprotein (HDL) cholesterol	54.27 ± 17.37
Triglycerides	112.79 ± 57.03
Glucose	105.50 ± 24.04
<b>Studied vessels (n = 480)</b>	
Left anterior descending artery	162 (33.75%)
Left circumflex coronary artery	144 (30.00%)
Right coronary artery	174 (36.25%)
<b>Medications at discharge</b>	
Aspirin	100 (53.77%)
ARB	32 (17.1%)
Beta-blockers	67 (35.8%)
ACE inhibitors	50 (26.7%)
Calcium channel blockers	28 (15.0%)
Statins	85 (45.5%)

BMI, body mass index; CAD: coronary artery disease; ARB, Angiotensin II Receptor Blockers; ACE, Angiotensin-converting enzyme. \* Clinical classification was based on European Society of Cardiology (ESC) guidelines [17].

From the 187 patients included in the current study, baseline geometries of 480 arteries were used for blood flow and LDL transport modeling. The final dataset included 174 RCAs, 162 LADs, and 144 LCXs. A total of 4000 3 mm segments were finally analyzed for baseline imaging characteristics, modeling results, and changes from baseline to follow-up. To our knowledge, this is the largest dataset, where blood flow and LDL transport modeling is performed for the prediction of atherosclerotic progression. A post-hoc power analysis was performed to calculate the power of our population for the prediction of atherosclerotic disease progression. We used an effect size  $f^2 = 0.135$  based on the calculation of  $r^2$ ;  $\alpha = 0.05$ ; total sample size of 187 patients (4000 arterial segments); max 15 tested predictors included in the final model for multiple linear regression analysis. Based on these, we observe

power = 0.90. A patient example with ESS and LDL concentration results is shown in Figure 2.

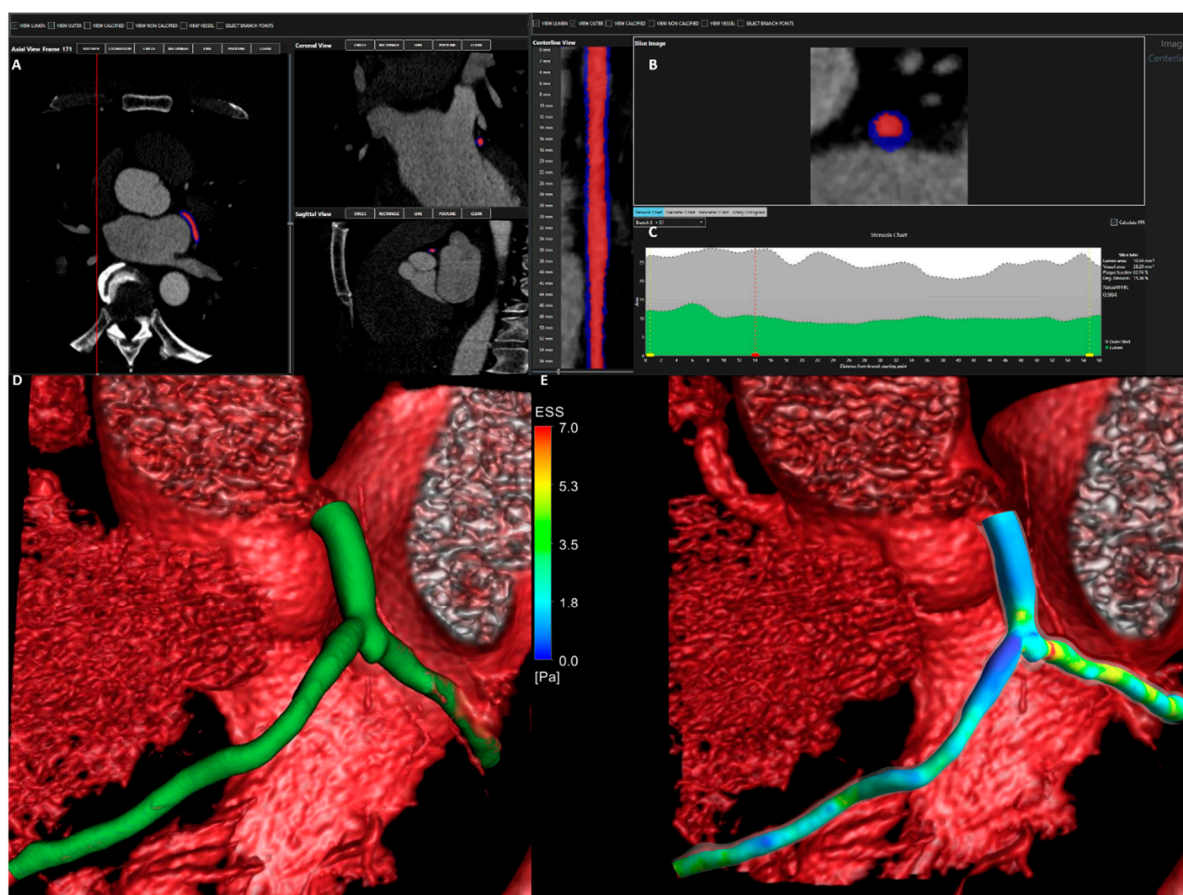


**Figure 2.** Example of a patient case as analyzed using the developed software. Panels A and B present the segmentation results, panel C shows the calculated SmartFFR for one branch, as well as metrics of lumen and wall area and plaque burden among the vessel's length. Panel D presents the reconstructed geometry back-projected on the coronary computed tomography angiography (CCTA) volume rendering and panel E shows the ESS distribution on the analyzed vessel.

Average values of imaging variables including lumen area, plaque volume and plaque burden for the 4000 analyzed coronary segments are reported for baseline and follow up CCTA scans in Table 2 together with computational modeling results at baseline.

### 3.1. Prediction of Plaque Progression

Overall plaque progression was defined for each 3 mm segment according to the presence of at least two of three conditions: reduction of lumen area by >20%, increase of plaque area by >20%, increase of plaque burden by >20%. Over the 4000 coronary segments analyzed, 1557 (39%) showed plaque progression. CCTA imaging and computational modeling data in segments without or with evidence of plaque progression are compared in Table 3.

**Table 2.** CCTA imaging variables at baseline and follow-up and results of computational modeling of endothelial shear stress (ESS), LDL concentration and calculation of SmartFFR at baseline.

	Baseline		Follow-Up		<i>p</i> -Value Baseline vs. Follow-Up	Delta		<i>p</i> -Value Baseline vs. Change between Follow-Up and Baseline
	Mean	Std. Dev.	Mean	SD		Mean	SD	
Lumen area (mm <sup>2</sup> )	6.86	3.89	6.34	3.90	<0.0001	−0.56	2.95	<0.0001
Plaque area (mm <sup>2</sup> )	7.16	4.30	7.29	4.62	<0.0001	0.14	4.41	<0.0001
Plaque burden	51.02	14.66	52.96	17.85	<0.0001	1.79	19.27	<0.0001
Minimum ESS (Pa)	1.78	2.36						
Normalized max. LDL concentration	0.24	0.12						
SmartFFR	0.89	0.12						

**Table 3.** Same variables as in Table 2 in segments without plaque progression (N = 1556) and with plaque progression (N = 2443).

		Baseline		Follow-up		<i>p</i> -Value Baseline vs. Follow-up	Delta		<i>p</i> -Value Baseline vs. Delta
		Mean	SD	Mean	SD		Mean	SD	
Segments with progression N = 1557	Lumen area (mm <sup>2</sup> )	7.47	3.92	5.74	3.75	<0.0001	−1.79	2.73	<0.0001
	Plaque area (mm <sup>2</sup> )	6.02	3.68	9.17	4.75	<0.0001	3.38	3.63	<0.0001
	Plaque burden	44.52	13.28	62.48	14.16	<0.0001	18.89	11.43	<0.0001
	Minimum ESS (Pa)	1.61	1.72						
	Normalized max. LDL concentration	0.24	0.12						
	SmartFFR	0.91	0.09						
Segments without progression N = 2443	Lumen area (mm <sup>2</sup> )	6.47	3.83	6.72	3.95	<0.0001	0.18	2.83	<0.0001
	Plaque area (mm <sup>2</sup> )	7.88	4.50	6.12	4.13	<0.0001	−1.81	3.62	<0.0001
	Plaque burden	55.16	13.99	47.04	17.35	<0.0001	−8.44	15.35	<0.0001
	Minimum ESS (Pa)	2.00	2.89						
	Normalized max. LDL concentration	0.24	0.12						
	SmartFFR	0.88	0.14						

At univariate linear regression analysis, older age, higher blood concentrations of triglycerides, and some specific lipid species (CE\_18\_3, CE\_20\_3, CE\_20\_4, PC\_36\_0, PC\_36\_3, TG\_54\_2, TG\_18\_1\_18\_18\_0, PS\_38\_6, PS\_40\_6, SM\_42\_1) were associated with plaque progression (Table 4). Among the baseline morphological and computational CCTA variables, lower plaque burden, lower minimum ESS, higher maximal LDL concentration, and higher SmartFFR were all associated with plaque progression. However, at multivariate linear regression analysis only age ( $p = 0.0067$ ) and lower baseline plaque burden ( $p < 0.0001$ ) remained independently associated with plaque progression. The univariate and multivariate logistic regression analysis for the prediction of plaque progression confirmed the previous results (Table 5).

**Table 4.** Univariate and multivariate linear regression analysis for association of relevant baseline clinical/biohumoral and CCTA variables with single components of plaque progression and their combination.

Dependent Variable	Effect	Univariate Linear Regression Analysis		Multivariate Linear Regression Analysis	
		Estimated Regression Coefficient (95% CI)	<i>p</i> -Value	Estimated Regression Coefficient (95% CI)	<i>p</i> -Value
Plaque progression (at least 2 out of 3 of the criteria below)	Age (years)	0.006 (0.000 to 0.012)	0.0429	0.011 (0.003 to 0.019)	0.0067
	Triglycerides (mg/dl)	0.001 (0.000 to 0.002)	0.0417	0.001 (−0.001 to 0.002)	0.2955
	CE_18_3 (μM)	0.003 (0.001 to 0.005)	0.0138	0.001 (−0.003 to 0.004)	0.7102
	CE_20_3 (μM)	0.008 (0.003 to 0.014)	0.0043	0.006 (−0.006 to 0.018)	0.3336
	CE_20_4 (μM)	0.002 (0.000 to 0.003)	0.0203	0.000 (−0.003 to 0.004)	0.7980
	PC_36_0 (μM)	0.009 (−0.001 to 0.018)	0.0845	-	-
	PC_36_3 (μM)	0.000 (−0.000 to 0.001)	0.0756	-	-
	TG_54_2_TG_18_1_18_18_0 (μM)	0.002 (−0.000 to 0.004)	0.0872	-	-
	PS_38_6 (μM)	0.169 (0.017 to 0.321)	0.0292	−0.128 (−0.374 to 0.118)	0.3046
	PS_40_6 (μM)	0.325 (−0.054 to 0.705)	0.0921	-	-
	SM_42_1 (μM)	0.002 (−0.000 to 0.005)	0.0892	-	-
	Baseline plaque burden	−0.012 (−0.013 to −0.011)	<.0001	−0.011 (−0.013 to −0.010)	<0.0001
	Minimum ESS (Pa)	−0.056 (−0.074 to −0.038)	<0.0001	0.004 (−0.004 to 0.011)	0.3653
	Maximum LDL concentration	0.075 (0.045 to 0.105)	<.0001	−0.004 (−0.033 to 0.024)	0.7593
	SmartFFR	0.385 (0.116 to 0.654)	0.0052	−0.027 (−0.379 to 0.326)	0.8816
Lumen area reduction by 20%	Diabetes Mellitus	−0.180 (−0.316 to −0.045)	0.0093	0.068 (−0.152 to 0.289)	0.5393
	Hypertension	−0.077 (−0.161 to 0.006)	0.0700	−0.101 (−0.229 to 0.028)	0.1221
	CE_16_0 (μM)	−0.000 (−0.000 to −0.000)	0.0330	−0.000 (−0.001 to 0.000)	0.5564
	CE_16_1 (μM)	−0.000 (−0.001 to 0.000)	0.0609	−0.000 (−0.001 to 0.000)	0.5856
	CE_18_1 (μM)	−0.000 (−0.000 to −0.000)	0.0439	0.000 (−0.000 to 0.000)	0.8448
	PS_36_1 (μM)	0.007 (−0.001 to 0.015)	0.0865	−0.000 (−0.001 to 0.001)	0.7504
	Baseline plaque burden	−0.006 (−0.007 to −0.006)	< 0.0001	−0.004 (−0.005 to −0.002)	<0.0001
	Minimum ESS (Pa)	−0.102 (−0.117 to −0.088)	< 0.0001	−0.021 (−0.027 to −0.014)	<0.0001
	Maximum LDL concentration	0.118 (0.093 to 0.142)	< 0.0001	0.057 (0.017 to 0.097)	0.0051
	SmartFFR	0.226 (0.011 to 0.441)	0.0394	0.087 (−0.219 to 0.394)	0.5720



**Table 5.** Univariate and multivariate binary logistic regression analysis for the plaque progression and lumen area decrease.

Dependent Variable	Effect	Univariate Logistic Regression Analysis		Multivariate Logistic Regression Analysis	
		Odds Ratio	<i>p</i> -Value	Odds Ratio	<i>p</i> -Value
Plaque progression	Age (years)	1.028 (1.001 to 1.056)	0.0401	1.067 (1.023 to 1.114)	0.0026
	Triglycerides (mg/dl)	1.004 (1.000 to 1.009)	0.0605	1.000 (0.992 to 1.009)	0.9453
	CE_16_1 (μM)	1.002 (1.000 to 1.004)	0.0650	1.002 (1.000 to 1.005)	0.0751
	CE_18_3 (μM)	1.011 (1.003 to 1.019)	0.0095	1.004 (0.979 to 1.030)	0.7523
	CE_20_3 (μM)	1.035 (1.011 to 1.060)	0.0043	1.021 (0.959 to 1.086)	0.5153
	CE_20_4 (μM)	1.006 (1.000 to 1.013)	0.0552	1.002 (0.982 to 1.023)	0.8269
	PC_36_0 (μM)	1.044 (0.999 to 1.091)	0.0534	1.025 (0.950 to 1.106)	0.5219
	TG_54_2_TG_18_1_18_1_18_0 (μM)	1.008 (0.999 to 1.016)	0.0783	1.009 (0.996 to 1.022)	0.1831
	PS_38_5 (μM)	1.512 (1.006 to 2.275)	0.0469	2.742 (1.116 to 6.734)	0.0278
	SM_38_1 (μM)	1.017 (0.999 to 1.034)	0.0581	1.032 (0.987 to 1.079)	0.1717
	SM_42_1 (μM)	1.012 (1.000 to 1.023)	0.0464	1.029 (1.005 to 1.054)	0.0168
	Baseline lumen area (mm <sup>2</sup> )	1.882 (1.493 to 2.371)	< 0.0001	1.171 (0.776 to 1.767)	0.4517
	Baseline plaque area (mm <sup>2</sup> )	2.613 (2.140 to 3.191)	< 0.0001	1.626 (1.117 to 2.366)	0.0112
	Baseline plaque burden	1.066 (1.053 to 1.079)	< 0.0001	1.066 (1.044 to 1.087)	<0.0001
	SmartFFR	5.671 (1.751 to 18.370)	0.0038	1.043 (0.773 to 1.407)	0.7814
	Minimum ESS (Pa)	1.194 (1.081 to 1.319)	0.0005	1.069 (0.737 to 1.550)	0.7239
	Maximum LDL concentration	1.164 (0.992 to 1.367)	0.0634	1.094 (0.170 to 7.038)	0.9245
Lumen reduction	Hypertension	1.570 (1.017 to 2.423)	0.0418	1.599 (1.025 to 2.495)	0.0385
	Age (years)	1.026 (1.001 to 1.052)	0.0436	1.001 (0.965 to 1.038)	0.9622
	Diabetes	2.025 (1.083 to 3.788)	0.0272	1.085 (0.514 to 2.289)	0.8305
	Hypertension	1.644 (1.029 to 2.626)	0.0377	3.116 (1.595 to 6.089)	0.0009
	Triglycerides (mg/dl)	1.004 (1.000 to 1.007)	0.0634	1.003 (0.996 to 1.010)	0.3980
	Cer_d18_1_16_0 (μM)	1.110 (0.985 to 1.250)	0.0859	1.192 (1.017 to 1.397)	0.0297
	CE_16_0 (μM)	1.001 (1.000 to 1.002)	0.0039	1.001 (0.998 to 1.004)	0.3945
	CE_16_1 (μM)	1.002 (1.000 to 1.003)	0.0077	1.000 (0.998 to 1.003)	0.7316
	CE_18_1 (μM)	1.001 (1.000 to 1.001)	0.0131	1.000 (0.999 to 1.002)	0.5703
	SM_36_2 (μM)	1.040 (1.000 to 1.081)	0.0513	1.148 (0.999 to 1.318)	0.0511
	SM_38_2 (μM)	1.080 (1.007 to 1.158)	0.0319	1.097 (0.855 to 1.408)	0.4665
	Baseline lumen area	2.904 (2.271 to 3.713)	<0.0001	1.974 (1.230 to 3.166)	0.0048
	Baseline plaque burden	1.038 (1.025 to 1.051)	<0.0001	1.018 (1.000 to 1.037)	0.0456
	SmartFFR	3.271 (1.103 to 9.704)	0.0327	1.399 (0.179 to 10.901)	0.7488
Minimum ESS (Pa)	1.656 (1.470 to 1.865)	<0.0001	1.516 (1.165 to 1.972)	0.0020	
Maximum LDL concentration	1.612 (1.341 to 1.938)	<0.0001	1.326 (0.864 to 2.034)	0.0014	

### 3.2. Prediction of Single Features of Plaque Progression

The association of clinical, biohumoral, and CCTA variables with single features of plaque progression (i.e., lumen area reduction, plaque area increase, and plaque burden increase) are also reported in Tables 4 and 5. Interestingly, baseline plaque burden and computational modeling results were all strongly associated with lumen area reduction. The binary logistic regression model showed that hypertension ( $p = 0.0009$ ), lower baseline plaque burden ( $p < 0.0456$ ), low ESS ( $p = 0.0020$ ) and the high accumulation of LDL ( $p = 0.0014$ ) are independent predictors of lumen reduction by  $> 20\%$ . The association results for plaque area and plaque burden change are also presented in Tables S1 and S2, with age and lower baseline plaque burden being the best predictors.

### 3.3. Interaction of ESS, LDL Concentration, and SmartFFR to Predict Plaque Progression

To assess the possible additional role of computational modeling in predicting overall plaque progression, a stepwise approach was followed, and for each model, the predictive accuracy, sensitivity, and specificity were calculated. The accuracy of a simple predictive model including age was 72%, but with zero sensitivity. The lipidomics based prediction accuracy, sensitivity, and specificity were 0.74, 0.38, and 0.93, respectively. Using only the imaging based features (morphological and computational results) accuracy, sensitivity, and specificity were significantly increased to 0.88, 0.92, and 0.81, respectively. Finally, the combination of all categories of features resulted in accuracy, sensitivity, and specificity of 0.88, 0.91, and 0.84, respectively. Figure 3 presents the ROC curve analysis comparing the effect of each different feature set.

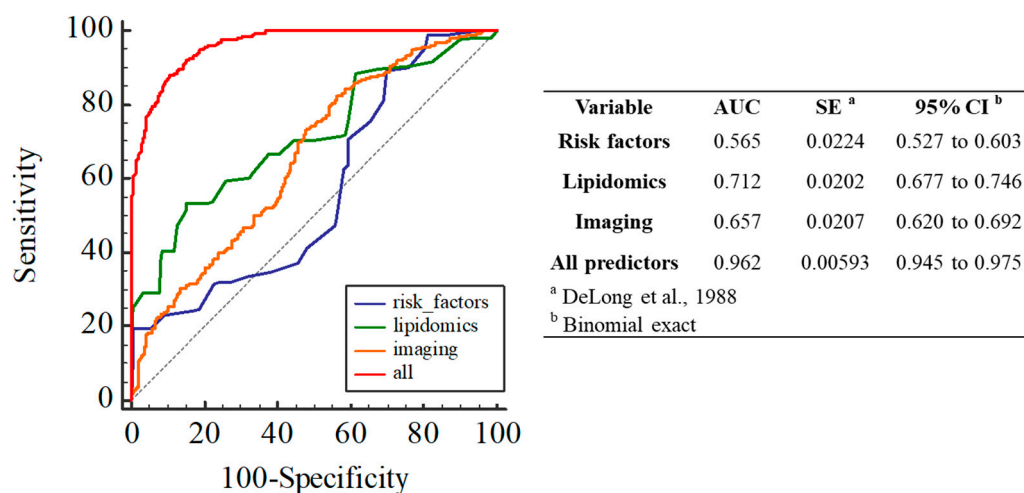


**Figure 3.** ROC curves of the risk score models comparing the predictive effect of each different feature sets.

## 4. Discussion

In the present study, we demonstrate that lipidomics in combination with computational modeling can be used for the prediction of atherosclerotic plaque progression. Overall plaque progression was defined when at least two out of the following three conditions occurred: 20% lumen reduction, 20% plaque increase, 20% plaque burden increase. In the current literature, there is not a fixed threshold for each of the three parameters to define the progression of an atherosclerotic plaque. Several studies have applied different thresholds ranging from around 10% to more than 20% change [6,18]; thus, using a conservative approach, we selected the highest threshold. In the current analysis, several cut-offs were examined considering that  $< 15\%$  was not investigated because it is questionable that CCTA can assess minor plaque change, and  $> 25\%$  was not examined because few patients present such disease progression. The cut-off of 20% presented the best balance between

the patients without (N = 1556) and with plaque progression (N = 2443) at 3 mm segment analysis. We performed 3D reconstruction of 480 main coronary vessels from 187 patients for blood flow and LDL transport modeling.

The results of the present study show that a lower baseline plaque burden coupled with a lower ESS and a higher LDL accumulation in the vessel wall are good predictors of coronary plaque progression, in particular of lumen coronary reduction >20% in a 6-year follow-up interval. CCTA, in combination with computational modeling, showed 88% accuracy for the prediction of plaque progression. Additionally, computational modeling affects the predictability of the results, since in most individual cases, a low minimum ESS or an increased accumulation of LDL at baseline are associated with plaque progression or lumen reduction. SmartFFR can also be used as an additional predictor, even if not independently associated at multivariate analysis.

Prediction of atherosclerotic plaque growth was attempted in previous studies, mainly based on invasive imaging modalities, where increased plaque burden at baseline and low ESS have been reported as independent predictors of plaque progression, in terms of lumen narrowing [3,19]. Those findings are partially in agreement with the present results. Low ESS was also a predictor of plaque progression in these studies, while baseline plaque burden showed the opposite results with our study. This discrepancy can be due to the specific characteristics of the SMARTool population, which included mainly patients with a low prevalence of obstructive CAD at enrolment. In this population, the majority of patients showing a relatively low coronary atherosclerotic burden were more likely to develop plaque progression. The incremental prediction value of biomechanical factors and ESS was already demonstrated [3,5,10].

CCTA efficacy and high cost-effectiveness is well known [20,21]. Its applicability and capacity to detect cardiovascular disease has been further improved recently by the introduction of advanced technology, allowing higher spatial and temporal resolution with increased imaging quality and reduced radiation exposure. Our study demonstrated that computational modeling of non-invasive coronary imaging by CCTA may allow accurate prediction of plaque progression without the need of invasive procedures and may warrant a cost-effective prevention of CAD. Studies focused on serial CCTA imaging to assess disease progression using blood flow simulation to estimate ESS have also demonstrated, in accordance with our findings, that low ESS is an independent predictor of lumen reduction or plaque burden increase [5,6]. The addition of the more advanced computational modeling of LDL transport and accumulation in the arterial wall increases the predictability results even more [10]. Our results were obtained in a larger population at medium–low risk and with a low prevalence of obstructive CAD. These patients could benefit most from an accurate non-invasive prediction of disease progression to target a preventive more aggressive medical treatment. Our results further support the argument that predictive models, including non-invasive evidence of low ESS, high concentration of LDL, and specific baseline morphological characteristics improve the prediction of plaque progression over traditional risk factors.

There is growing evidence that CCTA virtual FFR can be used as a substitute of invasive FFR for the functional assessment of coronary obstructive disease [21–23]. Our study demonstrates that non-invasive FFR can also be used as a predictor of disease progression and not only for diagnostic purposes. To our knowledge, this is the first time that non-invasive FFR is calculated in a serial patient database for prediction purposes, though the association of higher values of SmartFFR with plaque progression was not significant at multivariate analysis, a finding which possibly requires further investigation.

Finally, a novelty of this study is the inclusion of the patients' plasma lipidomics into the development of the predictive models. Previously, it was shown that several circulating lipid species are associated with the diagnosis of CAD and some species were also identified as biomarkers of disease progression [24]. Our work confirms that lipidomics can be used to predict plaque progression. Its combination with the morphological and computational CCTA parameters increased to 88% the predictive accuracy of the final model. In our work,

45.5% of the patients were under statins treatment. These patients were either dyslipidemic or obstructive CAD patients. Statin use was associated with an increased progression of calcified coronary plaque and a reduced progression of non-calcified coronary plaque as already reported for the whole SMARTool population [11]. Therefore, overall plaque area, plaque burden and lumen area changes were not significantly affected by statin use.

This work has some main limitations. First, about half of the population was under treatment with statins and all patients under antianginal and/or risk factor modifying medication during the follow-up period. Treatment is expected to variably affect plaque progression beyond baseline morphological and functional coronary features. Another limitation is that the threshold to define progression was selected arbitrary. In this study, we set the threshold considering the distribution of disease progression among the patients as well as previously selected cut-off values (6). Further work is needed with a reverse engineering analysis approach to identify the optimal threshold, which enables the prediction of disease progression with greater accuracy and reliability.

## 5. Conclusions

The possibility to predict the evolution of coronary atherosclerosis is highly relevant to ensure a safe and effective management of CAD patients in stable clinical conditions. More recently, predictive models based on CCTA imaging and computational results have been introduced to predict CAD progression. Traditional risk factors play a role on atherosclerosis progression at a systemic level, while site-specific hemodynamic conditions and lipid transport influence progression of single coronary plaques at a local level. Combining the two types of effects, our model was able to increase the predictive accuracy for coronary plaque progression to 88%. The proposed computational model could be used in the clinical practice as a prognostic decision support algorithm for the management of CAD using the outcomes to monitor effectively and non-invasively the patients with increased probability of CAD progression.

**Supplementary Materials:** The following are available online at <https://www.mdpi.com/2076-3417/11/5/1976/s1>, Annex 1. Chemical structures of lipids. Table S1. Univariate and multivariate linear regression analysis for association of relevant baseline clinical/biohumoral and CCTA variables with single components of plaque progression and their combination. Table S2. Univariate and multivariate binary logistic regression analysis for the plaque progression and lumen area decrease.

**Author Contributions:** Conceptualization, A.I.S., A.S., A.C., O.P., J.K., L.K.M., G.P., and D.I.F.; data curation, A.C., J.K., G.P., and S.R.; formal analysis, A.I.S., A.C., G.P., and S.R.; funding acquisition, G.P., S.R., and D.I.F.; investigation, A.I.S., A.S., D.N., J.K., L.K.M., G.P., and D.I.F.; methodology, A.I.S., P.T., V.K., P.S., N.T., and G.K.; project administration, S.R. and D.I.F.; resources, A.C., D.N., and J.K.; software, S.K.; supervision, A.I.S. and D.I.F.; validation, A.I.S.; visualization, A.I.S.; writing—original draft, A.I.S.; writing—review and editing, A.I.S., A.S., D.N., G.P., and D.I.F. All authors have read and agreed to the published version of the manuscript.

**Funding:** This work is partially funded by the European Commission: Project SMARTool, “Simulation Modeling of coronary ARtery disease: a tool for clinical decision support—SMARTool” (GA number: 689068). This work is partially funded by the European Commission: Project InSilc: in silico trials for drug-eluting BVS design, development, and evaluation (GA number: 777119).

**Institutional Review Board Statement:** Ethical approval was provided by each participating center (National Research Council, University of Turku, University of Zurich, Fondazione Toscana Gabriele Monasterio, Warsaw National Institute of Cardiology) through the approval of the clinical study by the Ethics Committee Vast Area Northwest of Tuscany (CEAVNO), Pisa, Italy, and all subjects gave written informed consent. Our clinical study follows the declaration of Helsinki.

**Informed Consent Statement:** Informed consent was obtained from all subjects involved in the study.

**Data Availability Statement:** No data are available due to ethics policies.

**Conflicts of Interest:** The authors declare no conflict of interest.

## References

1. Benjamin, E.J.; Virani, S.S.; Callaway, C.W.; Chamberlain, A.M.; Chang, A.R.; Cheng, S.; Chiuve, S.E.; Cushman, M.; Delling, F.N.; Deo, R.; et al. Heart Disease and Stroke Statistics-2018 Update: A Report from the American Heart Association. *Circulation* **2018**, *137*, e67–e492. [[CrossRef](#)] [[PubMed](#)]
2. Clemente, A.; Seitun, S.; Mantini, C.; Gentile, G.; Federici, D.; Barison, A.; Rossi, A.; Cuman, M.; Pizzuto, A.; Ait-Ali, L.; et al. Cardiac CT Angiography: Normal and Pathological Anatomical Features—A Narrative Review. *Cardiovasc. Diagn. Ther.* **2020**, *10*, 1918–1945. [[CrossRef](#)]
3. Stone, P.H.; Maehara, A.; Coskun, A.U.; Maynard, C.C.; Zaromytidou, M.; Siasos, G.; Andreou, I.; Fotiadis, D.; Stefanou, K.; Papafaklis, M.; et al. Role of Low Endothelial Shear Stress and Plaque Characteristics in the Prediction of Nonculprit Major Adverse Cardiac Events: The PROSPECT Study. *JACC Cardiovasc. Imaging* **2017**. [[CrossRef](#)] [[PubMed](#)]
4. Samady, H.; Eshtehardi, P.; McDaniel, M.C.; Suo, J.; Dhawan, S.S.; Maynard, C.; Timmins, L.H.; Quyyumi, A.A.; Giddens, D.P. Coronary Artery Wall Shear Stress Is Associated with Progression and Transformation of Atherosclerotic Plaque and Arterial Remodeling in Patients With Coronary Artery Disease. *Circulation* **2011**, *124*, 779–788. [[CrossRef](#)] [[PubMed](#)]
5. Sakellarios, A.; Bourantas, C.V.; Papadopoulou, S.L.; Kitslaar, P.H.; Girasis, C.; Stone, G.W.; Reiber, J.H.C.; Michalis, L.K.; Serruys, P.W.; de Feyter, P.J.; et al. The Effect of Coronary Bifurcation and Haemodynamics in Prediction of Atherosclerotic Plaque Development: A Serial Computed Tomographic Coronary Angiographic Study. *EuroIntervention* **2017**, *13*, e1084–e1091. [[CrossRef](#)]
6. Bourantas, C.V.; Papadopoulou, S.L.; Serruys, P.W.; Sakellarios, A.; Kitslaar, P.H.; Bizopoulos, P.; Girasis, C.; Zhang, Y.J.; de Vries, T.; Boersma, E.; et al. Noninvasive Prediction of Atherosclerotic Progression: The PROSPECT-MSCT Study. *JACC Cardiovasc. Imaging* **2016**, *9*, 1009–1011. [[CrossRef](#)] [[PubMed](#)]
7. Sakellarios, A.I.; Papafaklis, M.I.; Siogkas, P.; Athanasiou, L.S.; Exarchos, T.P.; Stefanou, K.; Bourantas, C.V.; Naka, K.K.; Michalis, L.K.; Parodi, O.; et al. Patient-Specific Computational Modeling of Subendothelial LDL Accumulation in a Stenosed Right Coronary Artery: Effect of Hemodynamic and Biological Factors. *Am. J. Physiol. Heart Circ. Physiol.* **2013**, *304*, H1455–H1470. [[CrossRef](#)]
8. Olgac, U.; Knight, J.; Poulidakos, D.; Saur, S.C.; Alkadhi, H.; Desbiolles, L.M.; Cattin, P.C.; Kurtcuoglu, V. Computed High Concentrations of Low-Density Lipoprotein Correlate with Plaque Locations in Human Coronary Arteries. *J. Biomech.* **2011**, *44*, 2466–2471. [[CrossRef](#)]
9. Tarbell, J.M. Mass Transport in Arteries and the Localization of Atherosclerosis. *Annu. Rev. Biomed. Eng.* **2003**, *5*, 79–118. [[CrossRef](#)]
10. Sakellarios, A.; Bourantas, C.V.; Papadopoulou, S.L.; Tsirka, Z.; de Vries, T.; Kitslaar, P.H.; Girasis, C.; Naka, K.K.; Fotiadis, D.I.; Veldhof, S.; et al. Prediction of Atherosclerotic Disease Progression Using LDL Transport Modelling: A Serial Computed Tomographic Coronary Angiographic Study. *Eur. Heart J. Cardiovasc. Imaging* **2016**. [[CrossRef](#)]
11. Smit, J.M.; van Rosendaal, A.R.; El Mahdiui, M.; Neglia, D.; Knuuti, J.; Saraste, A.; Buechel, R.R.; Teresinska, A.; Pizzi, M.N.; Roque, A.; et al. Impact of Clinical Characteristics and Statins on Coronary Plaque Progression by Serial Computed Tomography Angiography. *Circ. Cardiovasc. Imaging* **2020**, *13*, e009750. [[CrossRef](#)] [[PubMed](#)]
12. Liga, R.; Vontobel, J.; Rovai, D.; Marinelli, M.; Caselli, C.; Pietila, M.; Teresinska, A.; Aguade-Bruix, S.; Pizzi, M.N.; Todiere, G.; et al. Multicentre Multi-Device Hybrid Imaging Study of Coronary Artery Disease: Results from the Evaluation of INtegrated Cardiac Imaging for the Detection and Characterization of Ischaemic Heart Disease (EVINCI) Hybrid Imaging Population. *Eur. Heart J. Cardiovasc. Imaging* **2016**, *17*, 951–960. [[CrossRef](#)]
13. Siogkas, P.; Sakellarios, A.; Exarchos, T.P.; Athanasiou, L.; Karvounis, E.; Stefanou, K.; Fotiou, E.; Fotiadis, D.I.; Naka, K.K.; Michalis, L.K.; et al. Multiscale-Patient-Specific Artery and Atherogenesis Models. *IEEE Trans. Biomed. Eng.* **2011**, *58*, 3464–3468. [[CrossRef](#)] [[PubMed](#)]
14. Folch, J.; Lees, M.; Sloane Stanley, G.H. A Simple Method for the Isolation and Purification of Total Lipides from Animal Tissues. *J. Biol. Chem.* **1957**, *226*, 497–509. [[CrossRef](#)]
15. Wentzel, J.J.; Chatzizisis, Y.S.; Gijssen, F.J.; Giannoglou, G.D.; Feldman, C.L.; Stone, P.H. Endothelial Shear Stress in the Evolution of Coronary Atherosclerotic Plaque and Vascular Remodelling: Current Understanding and Remaining Questions. *Cardiovasc. Res.* **2012**, *96*, 234–243. [[CrossRef](#)] [[PubMed](#)]
16. Siogkas, P.K.; Anagnostopoulos, C.D.; Liga, R.; Exarchos, T.P.; Sakellarios, A.I.; Rigas, G.; Scholte, A.; Papafaklis, M.I.; Loggitsi, D.; Pelosi, G.; et al. Noninvasive CT-Based Hemodynamic Assessment of Coronary Lesions Derived from Fast Computational Analysis: A Comparison against Fractional Flow Reserve. *Eur. Radiol.* **2018**. [[CrossRef](#)]
17. Knuuti, J.; Wijns, W.; Saraste, A.; Capodanno, D.; Barbato, E.; Funck-Brentano, C.; Prescott, E.; Storey, R.F.; Deaton, C.; Cuisset, T.; et al. 2019 ESC Guidelines for the Diagnosis and Management of Chronic Coronary Syndromes. *Eur. Heart J.* **2019**. [[CrossRef](#)]
18. Bourantas, C.V.; Raber, L.; Sakellarios, A.; Ueki, Y.; Zanchin, T.; Koskinas, K.C.; Yamaji, K.; Taniwaki, M.; Heg, D.; Radu, M.D.; et al. Utility of Multimodality Intravascular Imaging and the Local Hemodynamic Forces to Predict Atherosclerotic Disease Progression. *JACC Cardiovasc. Imaging* **2019**. [[CrossRef](#)]
19. Stone, P.H.; Saito, S.; Takahashi, S.; Makita, Y.; Nakamura, S.; Kawasaki, T.; Takahashi, A.; Katsuki, T.; Nakamura, S.; Namiki, A.; et al. Prediction of Progression of Coronary Artery Disease and Clinical Outcomes Using Vascular Profiling of Endothelial Shear Stress and Arterial Plaque Characteristics The PREDICTION Study. *Circulation* **2012**, *126*, 172–181. [[CrossRef](#)]

20. Yamamoto, H.; Kihara, Y.; Kitagawa, T.; Ohashi, N.; Kunita, E.; Iwanaga, Y.; Kobuke, K.; Miyazaki, S.; Kawasaki, T.; Fujimoto, S.; et al. Coronary Plaque Characteristics in Computed Tomography and 2-Year Outcomes: The PREDICT Study. *J. Cardiovasc. Comput. Tomogr.* **2018**, *12*, 436–443. [[CrossRef](#)]
21. Norgaard, B.L.; Leipsic, J.; Gaur, S.; Seneviratne, S.; Ko, B.S.; Ito, H.; Jensen, J.M.; Mauri, L.; De Bruyne, B.; Bezerra, H.; et al. Diagnostic Performance of Noninvasive Fractional Flow Reserve Derived from Coronary Computed Tomography Angiography in Suspected Coronary Artery Disease: The NXT Trial (Analysis of Coronary Blood Flow Using CT Angiography: Next Steps). *J. Am. Coll. Cardiol.* **2014**, *63*, 1145–1155. [[CrossRef](#)] [[PubMed](#)]
22. Seitun, S.; Clemente, A.; Lorenzi, C.D.; Benenati, S.; Chiappino, D.; Mantini, C.; Sakellarios, A.I.; Cademartiri, F.; Bezante, G.P.; Porto, I. Cardiac CT Perfusion and FFR<sub>CTA</sub>: Pathophysiological Features in Ischemic Heart Disease. *Cardiovasc. Diagn. Ther.* **2020**, *10*, 1954–1978. [[CrossRef](#)]
23. Toia, P.; Grutta, L.L.; Sollami, G.; Clemente, A.; Gagliardo, C.; Galia, M.; Maffei, E.; Midiri, M.; Cademartiri, F. Technical Development in Cardiac CT: Current Standards and Future Improvements—A Narrative Review. *Cardiovasc. Diagn. Ther.* **2020**, *10*, 2018–2035. [[CrossRef](#)] [[PubMed](#)]
24. Kohno, S.; Keenan, A.L.; Ntambi, J.M.; Miyazaki, M. Lipidomic Insight into Cardiovascular Diseases. *Biochem. Biophys. Res. Commun.* **2018**, *504*, 590–595. [[CrossRef](#)] [[PubMed](#)]